### Title

Coupled Microenvironments for Artificial Photosynthesis of a C6 Oxygenated Product from CO2




### Journal

ACS Energy Letters, 11(2)

### ISSN

2380-8195



### Authors

Salazar, Matthew

Aitbekova, Aisulu

Yan, Katherine

et al.



### Publication Date

2026-02-13

### DOI

10.1021/acsenergylett.5c04064

10.1021/acsenergylett.5c04064

# Coupled Microenvironments for Artificial Photosynthesis of a $C_6$ Oxygenated Product from $CO_2$

Matthew Salazar[1,2‡], Aisulu Aitbekova[2,3‡], Katherine Yan[2,4,5‡], Dong Un Lee[2,4,5], Jonas C. Peters[1,2*], Thomas F. Jaramillo[2,4,5*], Harry A. Atwater[2,3*], Theodor Agapie[1,2*], Alexis T. Bell[2,6,7*]

[1]Division of Chemistry and Chemical Engineering, California Institute of Technology, Pasadena, CA 91125, USA

[2]Liquid Sunlight Alliance, California Institute of Technology, Pasadena, CA 91125, USA

[3]Department of Applied Physics and Materials Science, California Institute of Technology, Pasadena, CA 91125, USA

[4]SUNCAT Center for Interface Science and Catalysis, SLAC National Accelerator Laboratory, Menlo Park, CA 94025, USA

[5]Department of Chemical Engineering, Stanford University, Stanford, CA 94305, USA

[6]Lawrence Berkeley National Laboratory, Berkeley, CA 94720, USA

[7]Department of Chemical and Biomolecular Engineering, University of California, Berkeley, Berkeley, CA 94720, USA

[‡]Equal contributions

## ABSTRACT

Research on solar fuels generation has aspired to mimic photosynthesis. Powered by sunlight, photosynthesis converts $CO_2$ and water into $C_3$ intermediates en route to $C_6$ oxygenates (sugars). This study reports an analogous artificial photosynthesis process, inspired by the biological principle of an assembly of coupled microenvironments to achieve multi-step, selective chemical conversions to a desired $C_6$ product. Through four co-designed microenvironments working in concert, powered by simulated sunlight, this work demonstrates the conversion of $CO_2$ and water to 2-methyl-2-pentenal, a $C_6$ oxygenate. Specifically, a photovoltaic-driven electrolyzer with a Ag-Cu cathode converts $CO_2$ and water to $H_2$, CO, and $C_2H_4$. The products are fed into a photothermocatalytic reactor containing a dual-catalyst bed of Rh-$PPh_3$/SBA-15 and $TiO_2$, which

promotes ethylene hydroformylation to propanal, and subsequent propanal aldol condensation to 2-methyl-2-pentenal, a product convertible to hexane, a liquid fuel. This study presents an outline for co-designing assemblies of microenvironments that enable the conversion of $CO_2$ to $C_6$ products.

Solar-driven production of fuels and chemicals from $CO_2$ can play an important role in achieving an affordable, energy-secure, carbon-efficient economy with reduced emissions. Renewable energy-powered electrochemical $CO_2$ reduction ($CO_2R$) is a promising approach for converting waste $CO_2$ to chemical building blocks and fuels. However, the major products of $CO_2R$ are predominantly $C_1$ and $C_2$ products, e.g. CO, HCOOH, $CH_4$, $C_2H_4$ and $CH_3CH_2OH$, with a much lower selectivity towards $C_3$ products and beyond.[1-5] New pathways need to be developed to achieve the selective production of higher-chain carbon products, particularly for purely solar-powered processes. With this challenge in mind, this work draws inspiration from and aims to mimic photosynthesis, which takes $CO_2$, sunlight, and water to produce glucose, a $C_6$ product, and $O_2$ as a byproduct, through a series of tandem reactions within a highly organized assembly of coupled microenvironments (Scheme 1).

More broadly, several recent studies have produced higher carbon-number products (such as $C_{3+}$ products[6-10] and plastics[11]) by coupling $CO_2R$ and thermal systems in tandem. These systems use the gaseous outlet stream from a $CO_2R$ electrolyzer as the inlet to a thermocatalytic reactor. However, only a small number of these reported tandem systems are purely solar driven (or powered by simulated sunlight), and the higher carbon-number products are usually a mixture of hydrocarbons.[9, 12] Hence, a major challenge is to design a versatile approach to achieve selective chemical transformations in converting $CO_2$ and water vapor to a desired $C_{3+}$ molecular product using solar radiation as the only input energy source, much like natural photosynthesis.

To achieve this goal, requires co-design of an assembly of coupled microenvironments and the selection of appropriate operating conditions. We define "co-design" as the selection of components for each step such that the combination of components works as a system to achieve the targeted goal. The first step in the design sequence is selecting the chemical reactions needed to produce a $C_6$ product from $CO_2$ and $H_2O$ vapor, powered solely by solar radiation. As a design constraint, we chose to start the tandem system with the electrochemical reduction of $CO_2$ over a Cu-based catalyst, since it is known that this will produce a mixture of carbon-containing products

– CO, $C_2H_4$, $C_2H_5OH$ – together with $H_2$ that can be used to produce higher carbon number products by processes such as olefin oligomerization and hydroformylation. Since our earlier work had shown that ethylene dimerization over a Ni catalyst is poisoned by the presence of CO in the feed stream[9], we settled on coupling ethylene hydroformylation to produce propanal and subsequently aldol condensing propanal to 2-methyl-2-pentenal. The attractiveness of this scheme is that it makes use of $C_2H_4$, CO, and $H_2$, all of which are natural products of the electrochemical reduction of $CO_2$. We also chose to power the electrochemical cell using photovoltaic cells and to provide the energy needed for the thermally driven reactions, hydroformylation and aldol condensation by conducting these reactions in a photothermocatalytic reactor.[13]

Our design also aims to achieve high reaction rates, requiring high current densities of $CO_2R$, motivating the use of a membrane electrode assembly (MEA) electrolyzer. Pure $CO_2$ is fed to the cathode compartment, and electrolyte is fed to the anode compartment. $CO_2R$ occurs at the cathode catalyst/membrane interface with water transported through the membrane as the proton source. Since the rates of photothermally driven catalytic processes depend on the partial pressures of $H_2$, CO, and $C_2H_4$ exiting the MEA, these partial pressures of the components must be appropriately balanced. For example, the rate of hydroformylation of $C_2H_4$ to propanal is positive order in $H_2$ and $C_2H_4$ and inverse order in CO; however, the same is true for the competing but undesirable hydrogenation of $C_2H_4$ to ethane.[14] The selectivity between propanal and ethane is also dependent on temperature. Hence, the proper choice of reactant partial pressures and reaction temperature are necessary to achieve high propanal yields. The choice of catalysts used for photothermal catalytic processes is also critical, as they must exhibit adequate activity at temperatures attainable in photothermal reactors.[15-19] An additional consideration is the inhibitory effect of water vapor on photothermal catalysts, which can necessitate the removal of water from the products of $CO_2R$ before they enter into the photothermal reactor.[6, 20]

Here, we present an outline for the co-design of electrochemical and thermochemical microenvironments that can be assembled into a simulated solar-driven system that produces $C_{3+}$ products. Scheme 1 illustrates this system. In the first step, a photovoltaic-driven membrane electrode assembly (PV-MEA) is used to convert $CO_2$ and water into a gas stream containing CO, $H_2$, and $C_2H_4$. An Ag-Cu catalyst-deposited cathode is used to obtain an MEA outlet product composition well-suited for the subsequent photothermal catalytic processes – ethylene

hydroformylation to propanal, followed by aldol condensation to 2-methyl-2-pentenal. We achieved a total solar-to-chemical efficiency of 0.37±0.03 %, comparable in order of magnitude to the ~1% solar-to-chemical efficiency of natural photosynthesis.

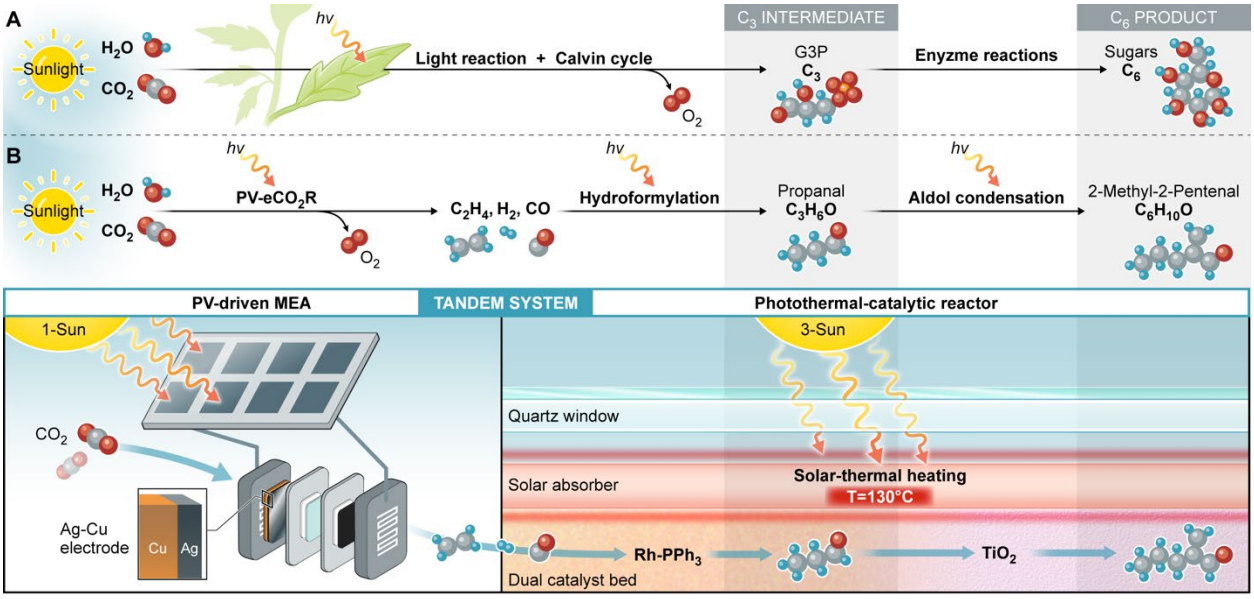


**Scheme 1.** Schematics of different solar-driven tandem systems. (A) Photosynthesis uses $CO_2$, sunlight, and water to produce G3P and $O_2$ via light reactions and the Calvin cycle. The G3P is used in enzyme catalyzed reactions to produce $C_6$ sugars like glucose. (B) The tandem system developed in this work converts $CO_2$, simulated sunlight, and water into a $C_6$ product via solar-driven electrochemical reduction of $CO_2$ to intermediates that are converted to the final product by photo-thermal catalysis. This multi-step process is accomplished by coupling a photovoltaically-driven membrane electrode assembly (MEA) electrolyzer to convert $CO_2$ and water into a mixture of CO, $H_2$, and $C_2H_4$ over the surface of Ag-Cu catalyst. The MEA outlet gas is dried by passage through a water adsorber and then fed to a dual-bed catalytic reactor heated by solar radiation. Propanal is produced in the first bed hydroformylation of ethylene over a supported rhodium hydroformylation catalyst promoted with triphenylphosphine ($PPh_3$) and 2-methyl-2-pentenal is produced in the second bed by aldol condensation of propanal over $TiO_2$.

$CO_2R$ was carried out using a commercially available MEA electrolyzer (Dioxide Materials; see SI for details) with cathode and anode areas of 5 $cm^2$. A PiperION membrane was used to separate the cathode and anode. The anode catalyst comprised $IrO_2$ nanoparticulate supported on carbon

paper (Sigracet). The cathode catalyst consisted of a 100 nm thick film of Cu (2.23 cm x 2.23 cm) deposited onto PTFE-treated carbon paper, onto which was deposited a 10 nm thick strip of Ag (6 mm x 2.23 cm) located at the inlet of the flow field (Figure S1a). Energy-dispersive X-ray spectroscopy (EDS) mapping confirms the presence of a uniformly deposited film of Ag on Cu that maintains its composition after $CO_2$ electrolysis (Figure S1b, c). The Ag strip enables efficient reduction of $CO_2$ to CO which is then carried downstream where it is adsorbs on Cu and is further reduced to $C_2H_4$.[21] This Ag-Cu electrode system was chosen to obtain a $H_2$, CO, $C_2H_4$ mixture suitable for subsequent hydroformylation of $C_2H_4$.

Galvanostatic experiments conducted at 1 atm demonstrated that the highest volume percentage of $C_2H_4$ was obtained by operating the MEA at a current density of $j_{geo}$ = -150 mA $cm^2$ (Table S1, S2) with a corresponding operating voltage of -3.6 V. For an inlet $CO_2$ flow rate of 10 ml/min, which produced the highest FE to ethylene (Figure S2), the single-pass conversion of $CO_2$ to $C_2H_4$ was 5.3% for Cu and 4.5% for Ag-Cu, whereas the molar ratios of $H_2$:CO:$C_2H_4$ was 2.3:2.1:1 for the Cu electrode and 4.8:1.7:1 for the Ag-Cu electrode (Figure 1 and Figure S3). While the CO:$C_2H_4$ ratios for Ag-Cu and Cu are comparable, the $H_2$:$C_2H_4$ ratio for Ag-Cu is roughly twice that for Cu. While a 1:1:1 molar ratio of $H_2$, CO, and $C_2H_4$ is stoichiometrically required for hydroformylation, we found that the rate of hydroformylation over Rh-$Ph_3$/SBA-15 (see below) was superior for higher $H_2$:$C_2H_4$ ratios (Figure S4). For this reason, all subsequent studies were carried out with the Ag-Cu catalyst.

Since the downstream photothermocatalytic process benefits from high pressure, we explored MEA operation at 5 atm using the Ag-Cu cathode catalyst. For comparison with the results obtained at 1 atm, the inlet flow rate was maintained at 10 mL/min at STP and the total current density was reduced to 120 mA/$cm^2$ with a cell voltage of –3.5 V (these conditions were chosen to match those used when the MEA was powered by PV cells, as discussed below). Under these conditions, outlet flow rate was 4.0 mL/min at STP. Operation of the MEA at 1 atm, with the same inlet flow rate and total current density, required a cell voltage was -4.0 V and resulted in an outlet flow rate of 5.7 mL/min. At 5 atm the single-pass conversion to $C_2H_4$ is 4.8 % and the ratio of $H_2$:CO:$C_2H_4$ is 1.8:3.4:1, whereas at 1 atm, the single-pass conversion to $C_2H_4$ is 3.9 % and the ratio of $H_2$:CO:$C_2H_4$ is 2.9:2.6:1 (**Figure 1b)**

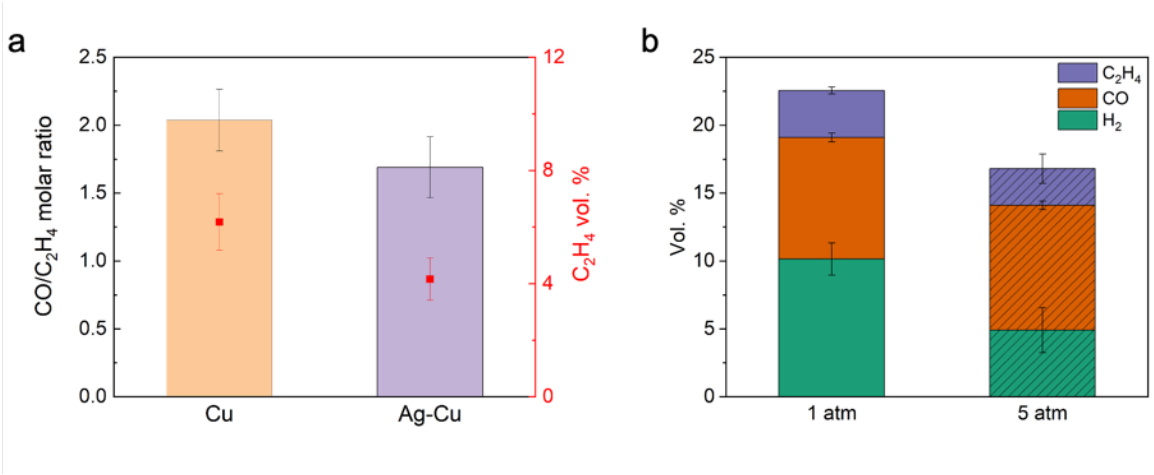


**Figure 1.** (a) Average molar ratios of CO:$C_2H_4$ for Cu and Ag on Cu tandem electrodes (Ag-Cu) measured under dark galvanostatic conditions at $j_{geo}$ = -150 mA $cm^{-2}$. Trials were 1 h in duration and error bars represent the standard deviation for triplicate measurements. (b) Average volume percent of gaseous products at 1 atm and 5 atm for Ag-Cu electrodes under dark galvanostatic conditions at $j_{geo}$ = -120 mA $cm^{-2}$ for 1 h. A $CO_2$ inlet flow rate of 10 mL/min was used for all experiments.

The heterogeneously catalyzed hydroformylation of $C_2H_4$ can produce propanal and 1-propanol (eq. 1 and 2). Propanal can be further converted to 2-methyl-2-pentenal via aldol condensation (eq. 3).

$C_2H_4 + CO + H_2 \rightarrow C_2H_5CHO$ (eq.1)

$C_2H_4 + CO + 2\,H_2 \rightarrow C_2H_5CH_2OH$ (eq. 2)

$2C_2H_5CHO \rightarrow C_6H_{10}O + H_2O$ (eq. 3)

$C_2H_4 + H_2 \rightarrow C_2H_6$ (eq. 4)

Ethane can be also produced by hydrogenation of $C_2H_4$ (eq. 4). Previous studies have shown that while supported Rh is a good catalyst for $C_2H_4$ hydroformylation, it suffers from poor selectivity due to competitive $C_2H_4$ hydrogenation.[6, 20] This problem can be suppressed by adding phosphine ligands to Rh, which increases the catalyst selectivity to $C_3$ oxygenates and suppresses the formation of ethane as a consequence of electron donation from the phosphine groups to Rh.[22-24]

To study the role of phosphine ligands on hydroformylation activity of Rh for $C_2H_4$ present in a $CO_2R$ product stream generated by the MEA, we synthesized a 1% Rh/SBA-15 catalyst and

functionalized it with 1,5-bis-(diphenylphosphino)pentane (L5) and triphenylphosphine ($PPh_3$) ligands.[22] We then compared the performance of the bare Rh/SBA-15 catalyst to functionalized samples (Rh-L5/SBA-15 and Rh-$PPh_3$/SBA-15) under a feed stream simulating the effluent from the MEA (2.7 vol. % $C_2H_4$, 4.9 vol. % $H_2$, 9.2 vol. % CO, $CO_2$ balance) (**Figure 2**) and compared the performance of the two functionalized catalysts under 12.3 vol. % $H_2$, 4.1 vol. % $C_2H_4$, 4.5 vol. % CO (Figure S5) under low ethylene conversion (< 1%). **Figure 2a** and **b** show that while Rh/SBA-15 and Rh functionalized with $PPh_3$ exhibit similar rates of propanal formation, the Rh/SBA-15 has a propanal selectivity of 40% and an ethane selectivity of 60%. The propanal selectivity is defined as the ratio of propanal formed to the total amount of propanal and ethane formed. On the other hand, Rh-$PPh_3$/SBA-15 exhibits a propanal selectivity of close to 90% and less than 10% ethane selectivity. This result demonstrates the efficiency of the phosphine ligand functionalization strategy to suppress undesired ethane formation even for dilute CO, $H_2$, $C_2H_4$ streams with $CO_2$ as a balance gas and a CO:$H_2$:$C_2H_4$ ratio different from the stoichiometric 1:1:1 ratio. Rh-L5/SBA-15 also showed a high propanal selectivity (Figure S5) but was less active compared to Rh-$PPh_3$/SBA-15. Therefore, our subsequent experiments were conducted on Rh-$PPh_3$/SBA-15.

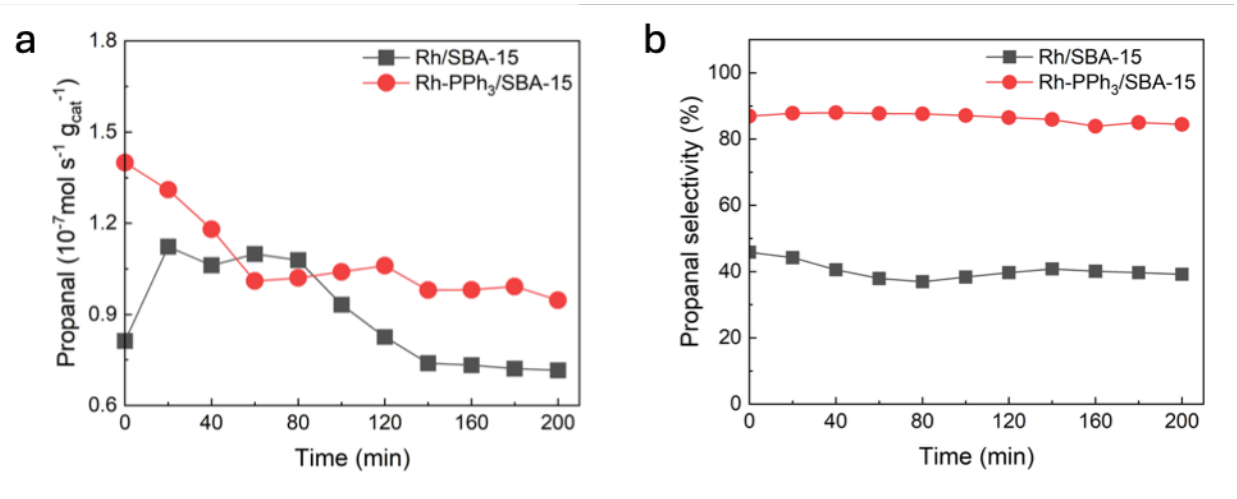


**Figure 2**. a-b) Propanal formation (a) and propanal selectivity (b) of Rh/SBA and Rh-$PPh_3$/SBA at 130˚C and 5 atm under feed conditions simulating the outlet of an MEA. The feed composition was 2.7 vol. % $C_2H_4$, 4.9 vol. % $H_2$, 9.2 vol. % CO, and $CO_2$ balance. The total flow rate was 62 mL/min. The mass of each catalyst was 100 mg. In panel b, the second reaction product was ethane.

With a hydroformylation catalyst selected, our next step was to investigate the effects of feed streams with excess $H_2$ and CO to understand the sensitivity of the catalyst to feed stream composition. We observed that increasing the $H_2$ concentration resulted in increased propanal production with no change to propanal selectivity (Figure S4), while increasing the CO concentration did not significantly change the selectivity nor the productivity of the Rh-$PPh_3$/SBA-15 catalyst (Figure S6). This sensitivity analysis informed our decision to select the Ag-Cu cathode for the MEA system.

We note that the gas mixture used for the experiments described above did not contain water vapor. The presence of water vapor was found to poison the hydroformylation activity of phosphine-promoted Rh catalysts (Figure S7). Since water is the proton source for the $CO_2R$ step, the outlet MEA stream contains water. To prevent the deactivation of the Rh catalyst, a packed-bed composed of silica gel desiccant was placed between the electrochemical and photothermocatalytic reactors. We did not observe a significant change in the MEA performance with the inclusion of the downstream water trap (Figure S8).

Following the successful generation of propanal from a dilute $CO/C_2H_4/H_2$ mixture, we sought to convert propanal to higher molecular weight products. We chose aldol condensation since this reaction can generate $C_6$ oxygenates from propanal (eq. 3).[25, 26] Titanium(IV) oxide ($TiO_2$) was selected as the catalyst since it catalyzes aldol condensation at mild temperatures (110-150 °C) and benefits from high operating pressure.[25] Given the matching temperature and pressure conditions of the ethylene hydrogenation reaction over the functionalized Rh catalyst and aldol condensation of propanal over $TiO_2$, we explored the possibility of carrying out both reactions sequentially by placing the two catalysts in series and performing both steps within a single reactor.

To test this concept, we assembled a dual-catalyst bed and evaluated its performance under feed conditions simulating the outlet of the MEA (2.7 vol. % $C_2H_4$, 4.9 vol. % $H_2$, 9.2 vol. % CO, $CO_2$ balance) in an externally heated reactor (Schematic S1). The effluent gas from the dual-catalyst bed reactor was sent to a condenser cooled in an ice bath to condense higher molecular weight products. The outlet from the condenser was analyzed online by gas chromatography, while the liquid from the condenser was analyzed by proton NMR at the end of the experiment. The whole

system was operated at 130 °C and 5 atm. Under these conditions, the dual bed produced propanal, and its concentration increased to 0.3 vol. % over the course of 5 h of time on stream (Figure S9), corresponding to 11% ethylene-to-propanal conversion. The propanal selectivity was greater than 90% with ethane as the second major product. In addition to gas-phase formation of propanal, we identified 2-methyl-2-pentenal via NMR in the liquid condensate. Using DMSO as an internal standard, we determined that the ethylene-to-2-methyl-2-pentenal conversion was 0.1 %.

To demonstrate the conversion of $CO_2$ and water vapor to 2-methyl-2-pentenal, we integrated the MEA and the photothermocatalytic reactor to form the solar-driven tandem system (Schematic 1, Schematic S2). The MEA was powered by two silicon solar panels (III-V Materials) each with dimensions 170 mm by 145 mm connected in parallel and irradiated under 1-sun (1000 W/m$^2$). The intersection of the intersection of the PV current-voltage curve and the electrolyzer polarization curve for this assembly resulted in a current density of 120 mA/cm$^2$ and a cell voltage of 4V, resulting in a power input of 2.4 W (Figure S10). The dual-catalyst bed was loaded into the photothermocatalytic reactor and was operated under 3-sun illumination (3000 W/m$^2$) to achieve a temperature of 130˚C and at a pressure of 5 atm.[15] As discussed above, to prevent the Rh-$PPh_3$ catalyst from poisoning by water present in the gas effluent stream of the MEA, we placed a water absorber between the MEA and the photothermocatalytic reactor. Operated at a total pressure of 5 atm, with 10 mL/min $CO_2$ (at STP) fed to the MEA, the flow rate of the gas outlet stream from the photothermocatalytic reactor was 6 mL/min (at STP) due to loss of $CO_2$ via membrane crossover in the MEA and the formation of liquid products. The solar-driven tandem system produced propanal (**Figure 3a**) with greater than 90 % selectivity (< 10 % selectivity to ethane). Major gas-phase products included $H_2$, CO, and $C_2H_4$ (**Figure 3b**). The higher propanal volume percentage in the tandem system compared to the dual-bed catalyst system, carried out using a simulated MEA outlet as the feed, is a consequence of using a lower total flow rate into the tandem system (10 vs 62 mL/min). The use of a higher total flow rate for the experiments carried out with the dual-bed catalyst system was necessitated by the minimum achievable flow rate for ethylene (1 mL/min). 2-methyl-2-pentenal was found in the liquid phase (Figures S11-12). The increase in propanal concentration overtime was attributed to the activation period observed for the based Rh catalysts.[22] The solar-to-chemical efficiency was calculated by dividing the heat of combustion of the desired products ($H_2$, CO, ethylene, propanal, and 2-methyl-2-pentenal) by the total solar

energy input (see SI for details). The overall solar-to-chemical efficiency was 0.37 ± 0.03%, with a solar-to-propanal efficiency of 0.06 ± 0.02% and solar-to-2-methyl-2-pentenal efficiency of 0.0022 ± 0.0008%. In comparison, the solar-to-biomass efficiency is ~1%. It should be noted that natural photosynthesis uses dilute $CO_2$ feedstocks (~400 ppm) and the solar irradiance is variable.[27, 28] The low energy efficiency for 2-methyl-2-pentenal is attributable to the low average production rate of this product (5 ± 2 x$10^{-10}$ mol/s), which was approximately 100x smaller than the propanal production rate (2.7 ± 0.9 x$10^{-8}$ mol/s). This finding shows that the efficiency bottleneck in the dual bed photothermal catalytic reactor is the aldol condensation step. Improving the efficiency of this step is the focus of future optimization. We performed an argon control experiment by operating the tandem system with an argon inlet feed. The only gaseous product detected was $H_2$, with a FE close to 100%, and no $C_6$ products were detected (Figure S13).

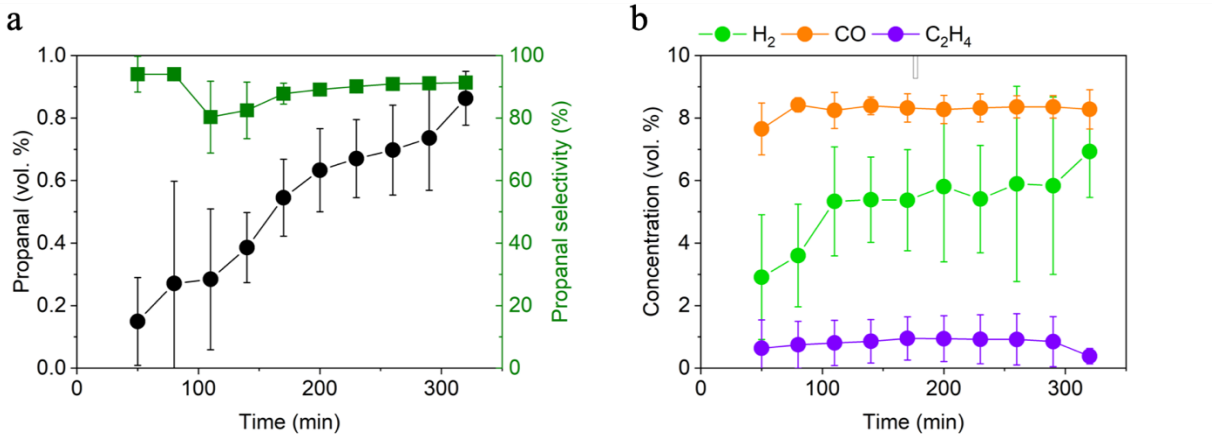


**Figure 3.** a) Propanal volume percent concentration in black circles and selectivity (defined with respect to ethane formed. See SI) in green squares versus time on stream for the solar-driven tandem system operated at 130 ˚C and 5 atm. b) Volume percent of $H_2$, CO, and $C_2H_4$ in the gas outlet stream from the solar-driven tandem system as a function of time on stream. The error bars represent the standard deviation for triplicate experiments.

We recognize that while this first demonstration offers room for improved performance and efficiency, the key outcome of the work is ultimately the demonstration of a design strategy and its implementation to mimic natural photosynthesis: we produce a $C_6$ product from $CO_2$ through a fully solar-driven process. Importantly, this approach of co-designing an assembly of coupled microenvironments is a versatile one, not restricted to 2-methyl-2-pentenal, a product readily

convertible to hexane, a liquid fuel. Selectivity to a wider range of possible products is achievable depending on design decisions involving the proper coupling of catalysts and solar-driven processes. This approach opens avenues to harnessing solar energy for the direct production of thousands of possible organic products that are key to modern industry.

In summary, the work reported here demonstrates that $C_3$ and $C_6$ products can be produced from $CO_2$ and $H_2O$ via strategic assembly of microenvironments in a tandem system comprised of a PV-MEA and a photothermocatalytic reactor driven exclusively by simulated solar energy. An Ag-Cu catalyst was used for the cathode in an MEA electrolyzer to generate a gas mixture of $CO/H_2/C_2H_4$ to feed into the downstream photothermocatalytic reactor. Using a simulated MEA outlet flow, we found that $C_2H_4$ can be converted to propanal with high selectivity over Rh-$PPh_3$/SBA-15. We also demonstrated that a dual-packed bed containing Rh-$PPh_3$/SBA-15 (to promote hydroformylation) and $TiO_2$ (to promote aldol condensation) produces 2-methyl-2-pentenal. For an inlet $CO_2$ flow rate of 10 mL/min at STP to the MEA and a total operating pressure of 5 atm, we achieved propanal and 2-methyl-2-pentenal production rates of $2.7 \pm 0.9 \times 10^{-8}$ mol/s and $5 \pm 2 \times 10^{-10}$ mol/s, with corresponding solar efficiencies of $0.06 \pm 0.02\%$ and $0.0023 \pm 0.0008\%$, respectively. These results provide an outline for the co-design of coupled microenvironments for targeted $C_6$ production from $CO_2$, $H_2O$, and sunlight. Further improvements could be achieved by optimizing MEA performance (i.e. increasing the electrode size and catalyst microenvironment) and enhancing the activity of the catalysts used for hydroformylation and aldol condensation. We also note that $H_2$ effluent from the tandem system could be used to hydrogenate 2-methyl-2-pentenal to hexane, a liquid fuel. In summary, the work reported here demonstrates that $C_3$ and $C_6$ products can be produced from $CO_2$ and $H_2O$ via strategic assembly of microenvironments in a tandem system comprised of a PV-MEA and a photothermocatalytic reactor driven exclusively by simulated solar energy.

**ACKNOWLEDGEMENTS**

This work was funded by the Liquid Sunlight Alliance, which is supported by the U.S. Department of Energy, Office of Science, Office of Basic Energy Sciences, Fuels from Sunlight Hub under Award Number DE-SC0021266. Part of this work was performed in the Stanford Nanofabrication Facility (SNF) and Stanford Nano Shared Facilities (SNSF), which are supported by the National

Science Foundation as part of the National Nanotechnology Coordinated Infrastructure under award ECCS-2026822. Part of this work was performed at the Caltech NMR facility. K.Y. acknowledges support from the U.S. Department of Energy, Office of Science, Office of Basic Energy Sciences, Chemical Sciences, Geosciences, and Biosciences Division, Catalysis Science Program through the SUNCAT Center for Interface Science and Catalysis, and the National Science Foundation Graduate Research Fellowship Program (DGE-2146755). A.A. acknowledges support by the Resnick Sustainability Institute. K.Y. acknowledges support of the NIH High End Instrumentation Grant (1 S10 OD028697-01) for NMR data. D.U.L. was supported by a cooperative research and development agreement sponsored by TotalEnergies American Services, Inc. (affiliate of TotalEnergies SE) under agreement number TC02307 for electrochemical performance evaluation and manuscript preparation.

## SUMMARY OF SUPPORTING INFORMATION

Description of experimental methods and materials, solar-to-fuel calculations of the tandem system, additional MEA data, experimental schematics, additional photothermal reactor data, control experiments, and product quantification.

## CORRESPONDING AUTHOR EMAILS:

Jonas C. Peters: jpeters@caltech.edu

Thomas F. Jaramillo: jaramillo@stanford.edu

Harry A. Atwater: haa@caltech.edu

Theodor Agapie: agapie@caltech.edu

Alexis T. Bell: alexbell@berkeley.edu

## REFERENCES


(1) Kuhl, K. P.; Cave, E. R.; Abram, D. N.; Jaramillo, T. F. New insights into the electrochemical reduction of carbon dioxide on metallic copper surfaces. *Energy & Environmental Science* **2012**, *5* (5), 7050-7059, 10.1039/C2EE21234J. DOI: 10.1039/C2EE21234J.

(2) Nitopi, S.; Bertheussen, E.; Scott, S. B.; Liu, X.; Engstfeld, A. K.; Horch, S.; Seger, B.; Stephens, I. E. L.; Chan, K.; Hahn, C.; et al. Progress and Perspectives of Electrochemical $CO_2$ Reduction on Copper in Aqueous Electrolyte. *Chemical Reviews* **2019**, *119* (12), 7610-7672. DOI: 10.1021/acs.chemrev.8b00705.

(3) Zhou, Y.; Martín, A. J.; Dattila, F.; Xi, S.; López, N.; Pérez-Ramírez, J.; Yeo, B. S. Long-chain hydrocarbons by $CO_2$ electroreduction using polarized nickel catalysts. *Nature Catalysis* **2022**, *5* (6), 545-554. DOI: 10.1038/s41929-022-00803-5.

(4) Sakamoto, N.; Sekizawa, K.; Shirai, S.; Nonaka, T.; Arai, T.; Sato, S.; Morikawa, T. Dinuclear Cu(I) molecular electrocatalyst for $CO_2$-to-$C_3$ product conversion. *Nature Catalysis* **2024**, *7* (5), 574-584. DOI: 10.1038/s41929-024-01147-y.

(5) Qi, K.; Zhang, Y.; Onofrio, N.; Petit, E.; Cui, X.; Ma, J.; Fan, J.; Wu, H.; Wang, W.; Li, J.; et al. Unlocking direct $CO_2$ electrolysis to $C_3$ products via electrolyte supersaturation. *Nature Catalysis* **2023**, *6* (4), 319-331. DOI: 10.1038/s41929-023-00938-z.

(6) Biswas, A. N.; Xie, Z.; Xia, R.; Overa, S.; Jiao, F.; Chen, J. G. Tandem Electrocatalytic–Thermocatalytic Reaction Scheme for $CO_2$ Conversion to $C_3$ Oxygenates. *ACS Energy Letters* **2022**, *7* (9), 2904-2910. DOI: 10.1021/acsenergylett.2c01454.

(7) Dodge, H. M.; Natinsky, B. S.; Jolly, B. J.; Zhang, H.; Mu, Y.; Chapp, S. M.; Tran, T. V.; Diaconescu, P. L.; Do, L. H.; Wang, D.; et al. Polyketones from Carbon Dioxide and Ethylene by Integrating Electrochemical and Organometallic Catalysis. *ACS Catalysis* **2023**, *13* (7), 4053-4059. DOI: 10.1021/acscatal.3c00769.

(8) Lee, M. G.; Li, X.-Y.; Ozden, A.; Wicks, J.; Ou, P.; Li, Y.; Dorakhan, R.; Lee, J.; Park, H. K.; Yang, J. W.; et al. Selective synthesis of butane from carbon monoxide using cascade electrolysis and thermocatalysis at ambient conditions. *Nature Catalysis* **2023**, *6* (4), 310-318. DOI: 10.1038/s41929-023-00937-0.

(9) Yap, K. M. K.; Aitbekova, A.; Salazar, M.; Kistler, T. A.; Rodríguez Pabón, M.; Su, M. P.; Watkins, N. B.; Lee, S.-W.; Agbo, P.; Weber, A. Z.; et al. $CO_2$ Conversion to Butene via a Tandem Photovoltaic–Electrochemical/Photothermocatalytic Process: A Co-design Approach to Coupled Microenvironments. *ACS Energy Letters* **2024**, *9* (9), 4369-4377. DOI: 10.1021/acsenergylett.4c01866.

(10) Zhang, J.; Kang, X.; Yan, Y.; Ding, X.; He, L.; Li, Y. Cascade Electrocatalytic and Thermocatalytic Reduction of $CO_2$ to Propionaldehyde. *Angewandte Chemie International Edition* **2024**, *63* (12), e202315777. DOI: https://doi.org/10.1002/anie.202315777.

(11) Zhelyabovskiy, M.; Jung, H.-J.; Diaconescu, P. L.; Peters, J. C.; Agapie, T. Plastic from CO2, Water, and Electricity: Tandem Electrochemical $CO_2$ Reduction and Thermochemical Ethylene-CO Copolymerization. *Angewandte Chemie International Edition* **2025**, *64* (24), e202503003. DOI: https://doi.org/10.1002/anie.202503003 (acccessed 2025/07/03).

(12) Schäppi, R.; Rutz, D.; Dähler, F.; Muroyama, A.; Haueter, P.; Lilliestam, J.; Patt, A.; Furler, P.; Steinfeld, A. Drop-in fuels from sunlight and air. *Nature* **2022**, *601* (7891), 63-68. DOI: 10.1038/s41586-021-04174-y From NLM.

(13) Su, M. P.; Aitbekova, A.; Salazar, M.; Williams, F. J.; Li, X.; Xiong, S.; Espinosa, M.; Peters, J. C.; Agapie, T.; Atwater, H. A. A photothermocatalytic reactor and selective solar

absorber for sustainable fuel synthesis. *Device* **2025**, *3* (3), 100604. DOI: https://doi.org/10.1016/j.device.2024.100604.
(14) Kiss, G.; Mozeleski, E. J.; Nadler, K. C.; VanDriessche, E.; DeRoover, C. Hydroformylation of ethene with triphenylphosphine modified rhodium catalyst: kinetic and mechanistic studies. *Journal of Molecular Catalysis A: Chemical* **1999**, *138* (2), 155-176. DOI: https://doi.org/10.1016/S1381-1169(98)00166-6.
(15) Su, M. P.; Aitbekova, A.; Salazar, M.; Williams, F. J.; Li, X.; Xiong, S.; Espinosa, M.; Peters, J. C.; Agapie, T.; Atwater, H. A. A photothermocatalytic reactor and selective solar absorber for sustainable fuel synthesis. *Device* **2025**, *3* (3), 100604. DOI: 10.1016/j.device.2024.100604.
(16) Bai, X.; Yuan, D.; Li, Y.; Song, H.; Lu, Y.; San, X.; Lu, J.; Fu, G.; Wang, S.; Ye, J. Ambient sunlight-driven photothermal methanol dehydrogenation for syngas production with 32.9 % solar-to-hydrogen conversion efficiency. *iScience* **2021**, *24* (2), 102056. DOI: https://doi.org/10.1016/j.isci.2021.102056.
(17) Fan, W. K.; Tahir, M. Recent developments in photothermal reactors with understanding on the role of light/heat for $CO_2$ hydrogenation to fuels: A review. *Chemical Engineering Journal* **2022**, *427*, 131617. DOI: https://doi.org/10.1016/j.cej.2021.131617.
(18) Ghoussoub, M.; Xia, M.; Duchesne, P. N.; Segal, D.; Ozin, G. Principles of photothermal gas-phase heterogeneous $CO_2$ catalysis. *Energy & Environmental Science* **2019**, *12* (4), 1122-1142, 10.1039/C8EE02790K. DOI: 10.1039/C8EE02790K.
(19) Song, C.; Liu, X.; Xu, M.; Masi, D.; Wang, Y.; Deng, Y.; Zhang, M.; Qin, X.; Feng, K.; Yan, J.; et al. Photothermal Conversion of $CO_2$ with Tunable Selectivity Using Fe-Based Catalysts: From Oxide to Carbide. *ACS Catalysis* **2020**, *10* (18), 10364-10374. DOI: 10.1021/acscatal.0c02244.
(20) Biswas, A. N.; Winter, L. R.; Xie, Z.; Chen, J. G. Utilizing $CO_2$ as a Reactant for $C_3$ Oxygenate Production via Tandem Reactions. *JACS Au* **2023**, *3* (2), 293-305. DOI: 10.1021/jacsau.2c00533.
(21) Chen, C.; Li, Y.; Yu, S.; Louisia, S.; Jin, J.; Li, M.; Ross, M. B.; Yang, P. Cu-Ag Tandem Catalysts for High-Rate $CO_2$ Electrolysis toward Multicarbons. *Joule* **2020**, *4* (8), 1688-1699. DOI: https://doi.org/10.1016/j.joule.2020.07.009.
(22) Huang, N.; Liu, B.; Lan, X.; Yan, B.; Wang, T. Promotion of diphosphine ligands ($PPh_2(CH_2)nPPh_2$, n = 1, 2, 3, 5, 6) for supported $Rh/SiO_2$ catalysts in heterogeneous ethene hydroformylation. *Molecular Catalysis* **2021**, *511*, 111736. DOI: https://doi.org/10.1016/j.mcat.2021.111736.
(23) Zakem, G.; Christopher, P. Active Site Entropy of Atomically Dispersed $Rh/Al_2O_3$ Catalysts Dictates Activity for Ethylene Hydroformylation. *ACS Catalysis* **2023**, *13* (8), 5502-5515. DOI: 10.1021/acscatal.2c06321.
(24) Zakem, G.; Ro, I.; Finzel, J.; Christopher, P. Support functionalization as an approach for modifying activation entropies of catalytic reactions on atomically dispersed metal sites. *Journal of Catalysis* **2021**, *404*, 883-896. DOI: https://doi.org/10.1016/j.jcat.2021.07.030.
(25) Martsinkevich, E. M.; Afaunov, A. A.; Flid, V. R.; Bruk, L. G. Heterogeneous catalytic condensation of propanal. *Russian Chemical Bulletin* **2021**, *70* (10), 2031-2033. DOI: 10.1007/s11172-021-3313-1.
(26) Sharma, S. K.; Parikh, P. A.; Jasra, R. V. Solvent free aldol condensation of propanal to 2-methylpentenal using solid base catalysts. *Journal of Molecular Catalysis A: Chemical* **2007**, *278* (1), 135-144. DOI: https://doi.org/10.1016/j.molcata.2007.09.002.

(27) Blankenship, R. E.; Tiede, D. M.; Barber, J.; Brudvig, G. W.; Fleming, G.; Ghirardi, M.; Gunner, M. R.; Junge, W.; Kramer, D. M.; Melis, A.; et al. Comparing Photosynthetic and Photovoltaic Efficiencies and Recognizing the Potential for Improvement. *Science* **2011**, *332* (6031), 805-809. DOI: doi:10.1126/science.1200165.
(28) Walker, D. A. Biofuels, facts, fantasy, and feasibility. *Journal of Applied Phycology* **2009**, *21* (5), 509-517. DOI: 10.1007/s10811-009-9446-5.